Full paper

High-performance near-field thermophotovoltaics for waste heat recovery

Bo Zhao[a], Kaifeng Chen[a], Siddharth Buddhiraju[a], Gaurang Bhatt[b], Michal Lipson[b], Shanhui Fan[a,*]

[a] Department of Electrical Engineering, Ginzton Laboratory Stanford University, Stanford, CA 94305, USA
[b] Department of Electrical Engineering, Columbia University, New York, NY 10027, USA

ARTICLE INFO

ABSTRACT

The US industries reject nearly 20–50% of the consumed energy into the environment as waste heat. Harvesting this huge amount of heat can substantially improve the energy usage efficiency. For waste heat in the medium temperature range ($\sim$ 500–900 K), traditional solid-state waste heat recovery techniques like thermoelectric generators and thermophotovoltaics (TPVs) are still suffering from relatively low efficiency or power density. In this work, we analyze a near-field TPV system consisting of a plasmonic emitter (indium tin oxide) and a narrow-bandgap photovoltaic cell (InAs) that are brought to deep sub-wavelength distances for high-efficiency and high-power-density waste heat recovery. We show that despite the inclusion of realistic nonradiative recombination rates and sub-bandgap heat transfer, such a near-field TPV system can convert heat to electricity with up to nearly 40% efficiency and 11 W/cm^2 power density at a 900 K emitter temperature, because of the spectral reshaping and enhancement by the thermally excited surface plasmons and waveguide modes. Thus, we show that for waste heat recovery, near-field TPV systems can have performances that significantly exceed typical thermoelectric systems. We propose a modified system to further enhance the power density by using a thin metal film on the cell, achieving a counterintuitively "blocking-assisted" heat transfer and power generation in the near-field regime.

1. Introduction

About 20–50% of the energy consumed in the US industries is rejected into the environment as waste heat in the form of hot exhaust gases, cooling water, and heat lost from hot equipment surfaces [1]. Harvesting this enormous amount of heat is thus of critical importance for improving the efficiency of energy usage and reducing carbon emissions. Currently, the most-widely used solid-state techniques for this purpose involve thermoelectric generators. Thermoelectric generators can typically provide power density on the order of 1 W/cm^2 from waste heat sources at medium temperature level ($\sim$ 500–900 K), but the efficiency is still relatively low (typically < 10%). Further improvement of their efficiency requires a development of new thermoelectric materials with high figures of merit, which is currently a very active area of research [2,3].

Thermophotovoltaics (TPVs) offer an interesting alternative solid-state approach for waste heat recovery [4]. A TPV system uses the waste heat to heat up an emitter. The thermal emission from the emitter is then converted to electricity via the photovoltaic effect. At present, the experimentally demonstrated efficiency of thermophotovoltaic systems is approaching 10% [5–10]. Moreover, there has been an extensive literature indicating that a higher system efficiency is possible

especially by controlling the thermal radiation from the emitter based on various nanophotonic designs [11–21]. Thus, the achievable system efficiency using TPVs should be at least quite competitive as compared to the thermoelectric approach.

The key challenge in using TPV for waste heat recovery then is to achieve high power density while maintaining efficiency. TPV using far-field radiative heat transfer has limited power density, since in the far field, only the propagating-wave channels can be used to transfer energy, and hence the heat transfer is fundamentally constraint by the blackbody limit. In the near-field regime where two objects are brought to a distance that is much smaller than the characteristic wavelength of the thermal radiation, the evanescent-wave channels can be used and the radiative heat transfer rate can be enhanced to orders of magnitude larger than the blackbody limit [22–35]. Near-field TPVs based on this effect have been demonstrated to possess enhanced efficiencies and power densities as compared to far-field TPVs [36–45].

For the temperature range for waste heat recovery, Ilic et al. [46] calculated that a near-field TPV system using an InAs cell and an indium tin oxide (ITO) emitter can yield an electric power density of 0.36 W/cm^2 with an efficiency of 12% at an emitter temperature of 600 K, due to the enhancement of near-field heat transfer from the surface plasmons of ITO. This analysis showed the great potential of

near-field TPV system for waste heat recovery. However, the calculation of Ilic et al. is idealized. For example, some of intrinsic non-idealities, including nonradiative recombination and the sub-bandgap heat transfer, were not taken into account. Since the effects of these non-idealities can be quite significant, it is important to provide a more realistic assessment of the performance of the near-field TPV system for waste heat recovery.

In this paper, we reexamine the near-field TPV system based on a plasmonic emitter (ITO) and a narrow-bandgap thin-film cell (InAs), taking into account the effects of nonradiative recombination in semiconductors and sub-bandgap heat transfer, in the context of recovering waste heat with a temperature around 900 K. The calculations are based on a detailed balance analysis and the formalism of fluctuational electrodynamics. We show that, with proper design, despite the inclusion of non-idealities, the power density and efficiency can significantly exceed what has been achieved in typical thermo-electric approaches. Also, unlike the idealized case considered in Ref. [46], in the presence of non-radiative recombination it is preferable to use a thin photovoltaic cell. We show that while the dominant enhancement effect comes from the thermally excited surface plasmon resonances, the waveguide modes in the thin cell play a significant role as well, especially at relatively large gap distances. Finally, we demonstrate that the power density can be further enhanced by placing a thin metal film on the cell. This is a somewhat counterintuitive result since one might think that the thin metal film might serve to block the near-field radiation.

The rest of the paper is organized as follows: In Section 2, we explain the theoretical models used to calculate the electric power and efficiency of the system. In Section 3, we discuss the performance of the proposed TPV system and the underlying physical mechanism. We evaluate the performance of the system when the emitter temperature changes between 500–1200 K. In Section 4, we discuss a modified system which contains a thin metal film on the cell. In Section 5, we summarize the findings of this work.

2. Theory and methods

We consider a near-field TPV system depicted in Fig. 1. ITO and InAs are the emitter and cell material, respectively. Heat is conducted from the heat source to the emitter, and the thermal radiation from the emitter is converted to electricity in the photovoltaic cell, with part of the heat dumped to the heat sink. A tungsten layer is used as the mechanical support of the ITO thin film, and it can also serve as a heat spreader to ensure uniform temperature in the ITO emitter. We take into account this tungsten layer in the electromagnetic modeling; it is modeled as infinitely thick in our calculation. The metal contact on the
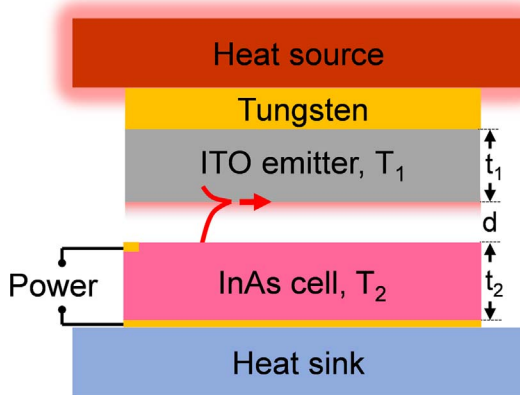

Fig. 1. Schematic of the near-field TPV system. The emitter is made of ITO and the cell is InAs. The temperatures of the ITO emitter and cell are T_1 and T_2, respectively. The thicknesses of the ITO emitter and InAs cell are t_1 and t_2, respectively, and the gap spacing between the emitter and cell is denoted by d.

backside of the InAs cell is modeled as a perfect mirror. In practice, one can use a metallic material that is reflective in the infrared range of interest. Such a mirror helps to recycle the low-energy photons and hence enhance the system efficiency [40]. The ITO emitter including the tungsten is assumed to be uniformly at temperature T_1. The cell is cooled by a heat sink and its temperature is maintained at T_2, which is assumed to be at 300 K in this work. The thicknesses of the ITO emitter and InAs cell are t_1 and t_2, respectively, and the gap spacing between the emitter and cell is denoted by d.

We calculate the performance of the system shown in Fig. 1 based on the detailed balance analysis [47]. The current density in the cell, J, is obtained by

$$J = q[F_{12}(0) - F_{21}(V) - R(V)] \tag{1}$$

where q is the elementary charge. In Eq. (1), R is the nonradiative recombination rate inside the cell and can be modeled by [48]

$$R(V) = (C_n n + C_p p)(np - n_i^2)t_2 + \frac{1}{\tau}\frac{np - n_i^2}{n + p + 2n_i}t_2 \tag{2}$$

In Eq. (2), n and p are the electron and hole concentrations, respectively, which depend on the voltage and the doping level. $n_i = 6.06 \times 10^{14}$ cm^{-3} is the intrinsic carrier concentration. $C_p = C_n = 2.26 \times 10^{-27}$ cm^6 s^{-1} are the Auger recombination coefficients. τ is the bulk Shockley-Read-Hall (SRH) lifetime. In this work, we assume an n-doped InAs cell with a doping level 2×10^{16} cm^{-3} and $\tau = 100$ ns [49].

In Eq. (1), F_{ij} denotes the number flux of photons with energy above the bandgap from body i to j, with the subscript 1 represents the emitter and 2 represents the cell. These photon fluxes are computed using the formalism of fluctuational electrodynamics [50,51], which results in

$$F_{ij} = \int_{\omega_c}^{\infty} \frac{\Theta(\omega, T_i, V_i)}{4\pi^2\hbar\omega}\left[\int_0^{\infty}\xi(\omega, \beta)\beta d\beta\right]d\omega \tag{3}$$

In Eq. (3), $\hbar$ is the reduced Planck constant, ω is the angular frequency, β designates the magnitude of the wavevector in the x-y plane, $\xi(\omega, \beta)$ is the photon tunneling probability (also called energy transmission coefficient), ω_c is the angular frequency corresponding to the bandgap of the cell, and $\Theta(\omega, T, V)$ is the expectation value of photon energy in a single mode at angular frequency ω

$$\Theta(\omega, T, V) = \frac{\hbar\omega}{\exp\left(\frac{\hbar\omega - qV}{k_B T}\right) - 1} \tag{4}$$

where k_B is the Boltzmann constant. V is the applied voltage and it is zero for the emitter. The photon tunneling probability includes contributions from both the transverse electric (TE) waves (s-polarization) and transverse magnetic (TM) waves (p-polarization), i.e., $\xi(\omega, \beta) = \xi_s(\omega, \beta) + \xi_p(\omega, \beta)$, where

$$\xi_j(\omega, \beta) = \begin{cases} \frac{(1 - |r_{1j}|^2)(1 - |r_{2j}|^2)}{|1 - r_{1j}r_{2j}e^{2ik_{z0}d}|^2}, & \beta < k_0 \\ \frac{4[\text{Im}(r_{1j})\text{Im}(r_{2j})]e^{-2|k_{z0}|d}}{|1 - r_{1j}r_{2j}e^{2ik_{z0}d}|^2}, & \beta > k_0 \end{cases} \tag{5}$$

with j denoting either s or p polarization. In Eq. (5), r_{1j} and r_{2j} are the reflection coefficients of the emitter and cell, respectively, and Im takes the imaginary part [52]. The magnitude and the z-component of the wavevector in vacuum are denoted as k_0 and k_{z0}, respectively. We note that Eq. (5) contains the contribution of the propagating waves ($\beta < k_0$) and the evanescent waves ($\beta > k_0$). In the far field, only the propagating waves contribute to the power transfer, but the evanescent waves contribute dominantly in the near-field regime.

The heat transfer rate (denoted by E below) has contributions both from frequency components above the bandgap due to electronic excitations (E^e), and from frequency components below the bandgap due to phonon-polariton excitations (E^p), i.e., $E = E^e + E^p$, with

$$E^e = \frac{1}{4\pi^2} \int_{\omega_c}^{\infty} [\Theta(\omega, T_1, 0) - \Theta(\omega, T_2, V)] \left[\int_0^{\infty} \xi(\omega, \beta)\beta d\beta \right] d\omega \tag{6}$$

$$E^p = \frac{1}{4\pi^2} \int_0^{\omega_c} [\Theta(\omega, T_1, 0) - \Theta(\omega, T_2, 0)] \left[\int_0^{\infty} \xi(\omega, \beta)\beta d\beta \right] d\omega \tag{7}$$

Eqs. (6) and (7) contain double integrations over ω and β. We obtain the spectral heat flux by integrating only over β. The power density and the efficiency of the system are defined as

$$P = JV \tag{8}$$

and

$$\eta = \frac{P}{E^e + E^p} \times 100\% \tag{9}$$

These two equations are used to maximize P and η with respect to V. In general, the maximum P and η are achieved at different voltages.

For a high-performance TPV system, we desire a high spectral heat transfer right above the bandgap of the cell. It is well known that surface resonances can significantly enhance near-field heat transfer [36,37,46]. In this work, we choose InAs, which is commonly used for TPV system, as the photovoltaic cell. The optical properties of InAs, as well as tungsten as shown in Fig. 1, are obtained from Ref. [53]. Since the bandgap energy of InAs is at 0.354 eV at 300 K, infrared plasmonic emitters such as transparent conductive oxides [54], which support surface resonances that are slightly above this energy, would be a potentially good choice for the emitter. We use ITO in this work for its wide availability and high-temperature stability (up to 1400 °C) [55]. The dielectric constant of ITO is modeled by a free-electron Drude model $\varepsilon(\omega) = \varepsilon_{\infty}(1 - \omega_p^2/(\omega^2 + i\omega\Gamma))$, where $\varepsilon_{\infty} = 4$, $\omega_p = 0.4 - 0.9$ eV, and $\Gamma = 0.1 - 0.15$ eV [56]. Note that the plasma frequency and damping rate is tunable by controlling the amount of oxygen during deposition, which offers a degree of freedom to optimize the performance of the TPV system. On the interface of semi-infinite ITO and vacuum, there is a strong surface plasmonic resonance, which is p-polarized, at the frequency when the real part of ε, i.e., $Re(\varepsilon)$, approaches -1. This frequency can be estimated as $\omega_{res} \approx \sqrt{\varepsilon_{\infty}/(\varepsilon_{\infty} + 1)}\omega_p$, which is about $0.9\omega_p$ for ITO. In this work, we therefore choose an ITO plasma frequency $\omega_p = 0.5$ eV, such that the surface resonance frequency, at 0.44 eV, is slightly above the bandgap of InAs. Such an ITO layer has a relaxation rate of $\Gamma = 0.1$ eV.

3. Performance of ITO-InAs near-field TPV

We first focus on optimizing the structure for a heat source at a temperature $T_1 = 900$ K. We find that P and η increase with the ITO film thickness t_1 and become insensitive to t_1 once $t_1 > 30$ nm. Thus, we set $t_1 = 30$ nm in this work. As to the cell thickness t_2, a thicker cell has a higher absorption but also higher non-radiative recombination, as can be seen in Eq. (2). Thus, once the nonradiative recombination is taken into account the cell thickness needs to be optimized. In addition, previous studies suggest that thin-film cells can support waveguide modes that enhance the absorption in the cell [41]. In our simulations, we vary t_2 between 0.1 and 3 μm to find the cell thickness that maximizes P or η. Fig. 2 displays the maximum P and η at different gap distances. The optimized t_2 for P is shown in the inset. At $d = 10$ nm, P reaches 11 W/cm^2, which significantly exceeds typical thermoelectric systems operating in this temperature range [2], and is comparable to the state-of-the-art thermoelectric systems [57]. On the other hand, the maximum efficiency of this system, at nearly 40%, is significantly higher than the maximum efficiency of the currently available thermoelectric systems. We note that the efficiency at the maximum power point is 39.3%, quite close to the maximum efficiency point.

In order to analyze the mechanism responsible for such high performance, we show the spectral heat flux including the contribution from both s- and p-polarizations at the maximum power P at $d = 10$ nm
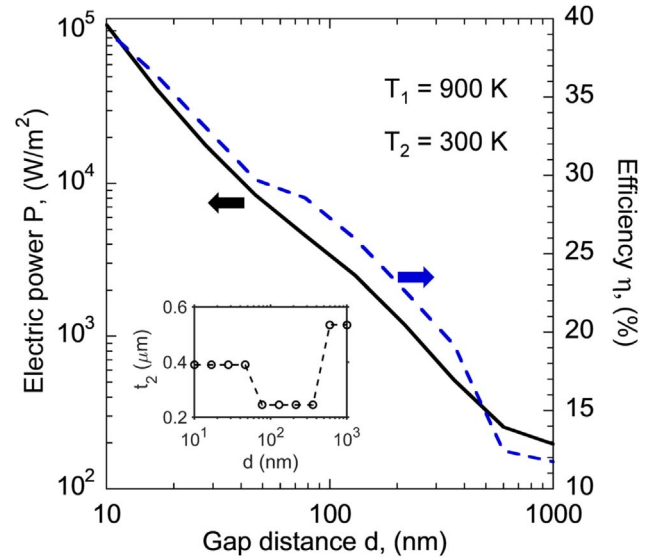

Fig. 2. Maximum electric power and efficiency of the near-field TPV at $T_1 = 900$ K. The inset shows the cell thickness at the maximum P for each gap distance.
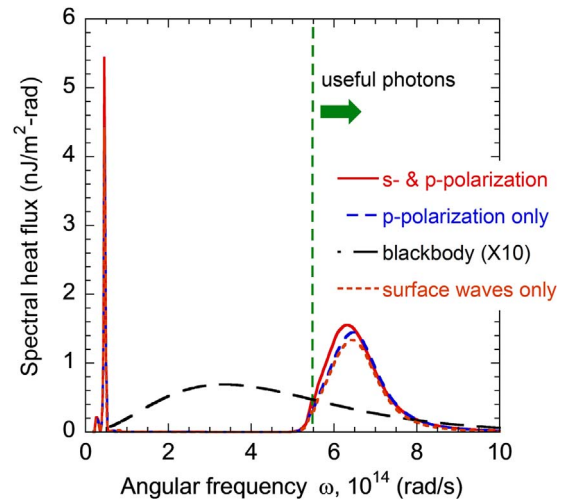

Fig. 3. Spectral heat flux at the maximum electric power density for the near-field TPV at $d = 10$ nm and $T_1 = 900$ K. The bandgap of InAs is $\omega_c = 5.5 \times 10^{14}$ rad/s and is marked using a vertical dashed line on the plot.

and $T_1 = 900$ K in Fig. 3. Compared to the far-field blackbody spectrum, the spectral heat flux in the near field is significantly enhanced and redistributed in the near field. There is a spectral peak slightly above the bandgap, from which the power is produced. Another heat transfer peak exists below the bandgap around 0.45×10^{14} rad/s that does not contribute to power generation and therefore is parasitic.

The physical origins of these two peaks are better illustrated by examining the transmission coefficient (ξ in Eq. (3)) as a function of ω and β, as shown in Fig. 4(a) and (b). The bright color indicates a high transmission coefficient. The green dashed lines are the light lines of vacuum and InAs, respectively. Note that due to the sum of both s and p polarizations the maximum transmission coefficient is 2.

In the above-bandgap frequency range, InAs exhibits significant absorption since it is a direct band gap material. Both the waveguide modes in the InAs film [41,44] and the SPPs on the interface of ITO and vacuum are excited as indicated by the bright bands. The dispersion curve of the SPPs is overlaid on the plot to further justify the interpretation of one of the resonances as the SPP from the ITO layer. Thus, both the waveguide modes and the SPPs contribute to the above-bandgap peak in Fig. 2.
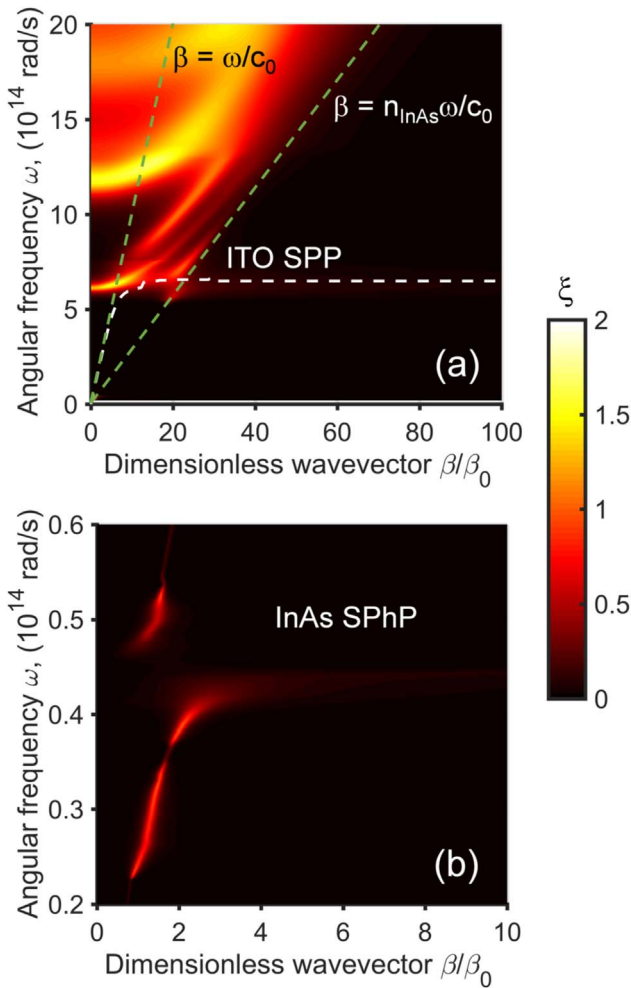
Fig. 4. Transmission coefficient as a function of ω and β for the near-field TPV system when $d = 10$ nm. (a) is for a high-frequency spectral range and (b) is for a low-frequency spectral range. The green dashed lines are the light lines of vacuum and InAs, and the white dashed line is the dispersion of the SPP on the ITO-vacuum interface. Wavevector β is normalized by $\beta_0 = \omega_0/c_0$ with $\omega_0 = 10^{14}$ rad/s and c_0 the speed of light in vacuum.

To further analyze the role of the ITO SPPs, we separate the contribution from the s- and p-polarizations. The surface modes are p-polarized [36,37] and the waveguide modes can be excited for both polarizations [41]. The blue dot-dashed curve in Fig. 3 shows the spectral heat flux contributed by p-polarization waves only. The spectrum is very similar to the spectrum that contains contributions of both polarizations, indicating that the dominating contribution is from the p-polarized modes. To further separate the contribution of the surface modes from that of the waveguide modes, we evaluate the spectral heat flux by setting the lower bound of the integration of β to $n_{InAs}\omega/c_0$. By doing this, the waveguide modes are excluded from the integration. The obtained spectral heat flux is shown in Fig. 3 as the orange dashed line. The small difference between the spectra with and without the contributions from the waveguide modes indicates that the surface resonances dominate the above-bandgap spectral heat flux peak. This can be understood since the wavevector β of the waveguide modes are limited by the refractive index of InAs (n_{InAs}) but the wavevector of the ITO SPPs are not thus limited and can be much larger near ω_{res}, resulting in an enhanced spectral heat flux based on Eq. (6). Therefore, even though a thin cell is used in this system, at the gap spacing of 10 nm, the waveguide mode does not play a significant role in the near-field heat transfer, in contrast with some of the previous works using thin cells where waveguide modes play a more significant role [41,44]. We note that, however, the contribution of the ITO SPPs decays faster

compared to the waveguide modes as the gap spacing increases, and therefore, the waveguide modes can be dominant at larger gap distances. For example, at $d = 100$ nm, the waveguide mode contributes more than 90% of the above-bandgap heat transfer, though the power density P drops to about 0.25 W/cm^2.

In the frequency range below the InAs band gap, the heat flux peak around 0.45×10^{14} rad/s is induced by the surface phonon polaritons (SPhPs) of InAs as can be identified in Fig. 4(b). Since InAs is a polar material, the real part of the dielectric function goes from positive to negative around the optical phonon frequency. At the frequency where Re(ε) is close to -1 (not exactly -1 because of the effect of the ITO emitter [58]), the SPhPs can be excited and contribute significantly to heat transfer [21]. We perform a spectral integration in the spectral region at the vicinity of SPhPs. It turns out that over 10% of the heat flux is contributed by the SPhPs, though the spectral peak is relatively narrow. We note that the wave vectors of SPPs are much larger compared to that of SPhPs. Therefore, when the gap distance decreases, the contribution of SPPs increases faster than SPhPs, and the above-bandgap heat transfer increases by a larger amount than the below-bandgap parasitic heat transfer does. The efficiency and electrical power thus both increase with reducing gap distance.

To evaluate the performance of the proposed system at different temperatures, we show in Fig. 5(a) and (b) the maximum electric power and efficiency of the system when T_1 is between 500 K and 1200 K, respectively. In the calculation, the thickness of the cell is fixed at 0.39 μm based on the optimized results in Fig. 2. Since the photon energy distribution changes based on Eq. (4), the optimized plasma frequency for the emitter also changes as a function of temperature. We fix Γ at 0.1 eV but allow ω_p to change between 0.4 and 0.9 eV in the calculation. The maximum P and η of the system increase as the temperature increases. The maximum values are 54 W/cm^2 and 47% at 1200 K with a 10-nm gap spacing. Therefore, near-field TPVs can be very promising for waste heat recovery under high operating temperatures where one cannot use thermoelectric generators [3,57]. The efficiency falls below 10% for $T_1 = 500$ K even at $d = 10$ nm gap spacing because of the significant contribution from parasitic heat transfer due to the phonon-polariton of InAs [21]. The power density drops to below 0.1 W/cm^2. To improve the performance for this low-temperature range, we may apply similar designs but use a narrower-bandgap semiconductor such as InSb, together with a plasmonic material with a lower plasma frequency [46].

Ref. [46] analyzed this system in the absence of nonradiative recombination, and obtained an optimal power of $P = 0.36$ W/cm^2 and efficiency $\eta = 12\%$, when the emitter temperature T_1 is set at 600 K. (We were able to reproduce this result in our model by taking into account only the contributions of the p-polarizations. Taking into account both polarizations further bring down the efficiency to 9% since the sub-bandgap heat transfer also has substantial contributions from the s-polarizations.) In contrast, in Fig. 5(a) and (b), we show that this system can achieve an optimal power of $P = 0.45$ W/cm^2 and efficiency $\eta = 15.3\%$, even after we take into account the nonradiative recombination. The higher efficiency and power density is achieved by tuning the plasma frequency of the ITO, and also by tuning the thickness of the InAs layer.

Fig. 5(c) shows the optimized plasma frequency for the ITO at different emitter temperatures and gap distances. In general, the optimized plasma frequency shifts to higher values at higher temperatures. For $d = 10$ nm, since the dominant contribution is from the surface waves, it is better to have the surface plasmon frequency to be just above the bandgap and hence the choice of the plasma frequency shows a weaker temperature dependency as compared to larger gap spacing.

4. Power density enhancement with a thin Pt layer on top of the cell

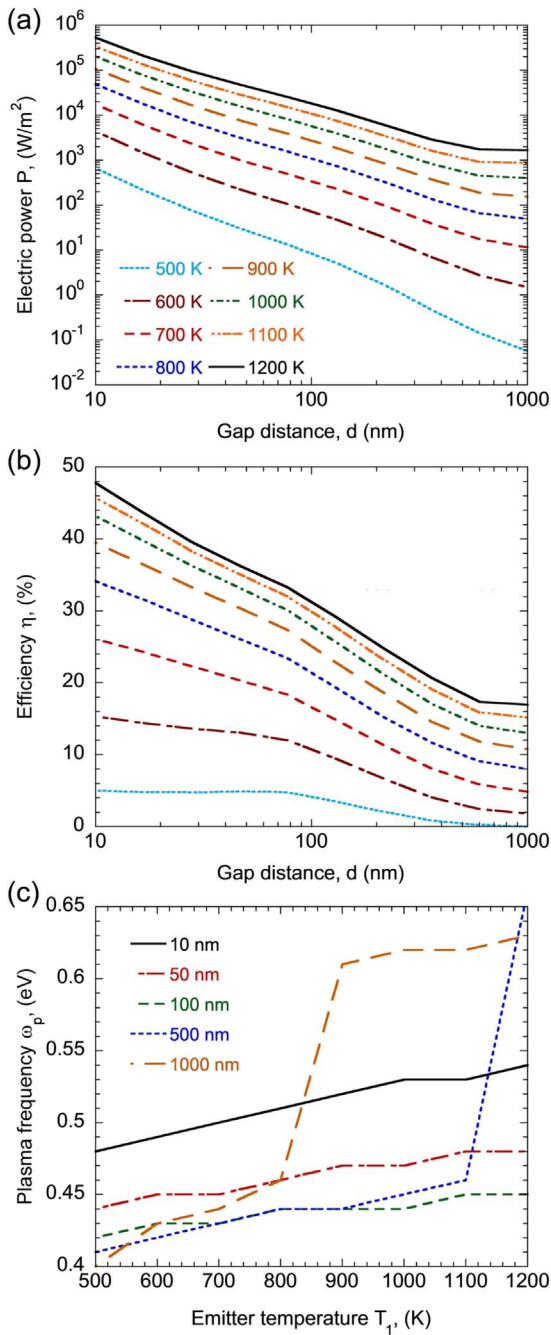Based on the near-field TPV configuration as considered above, we

Fig. 5. (a) Maximum power and (b) efficiency of the near-field TPV at different gap spacing. (c) The optimized plasma frequencies at different emitter temperatures and gap distances.

propose a modification to further improve the power density. Since the absorption in the cell is proportional to $|\mathbf{E}|^2$, where $\mathbf{E}$ is the electric field in the cell, to improve the power density it is preferable to have a larger E-field in the cell. We note that the SPPs on the interface of ITO and vacuum are evanescent because of the large parallel wavevectors, and thus the mode profile decays exponentially away from the emitter surface (as indicated in Fig. 1). Since the cell is away from the ITO surface, only the evanescent tail of the modal electric field of the SPP contributes to the enhancement of the absorption in the cell. To fully take advantage of the strong electric field intensity associated with surface resonances, it is instead preferable to create surface resonances as close to the cell as possible. Here, we propose to simply use a thin metal layer to cover the cell to achieve this goal. This may be

counterintuitive since one might think that a metal layer would be highly reflective in the far field and thus suppresses the absorption in the cell. Here a very thin layer is used such that the reflection effect is not very significant and one can achieve a strong near-field enhancement.

The inset in Fig. 6(a) shows a schematic of the modified near-field TPV. We use a 2-nm platinum (Pt) to cover the InAs cell because Pt film has a relatively lower plasma frequency compared to other noble metals like Ag and Au, and such a thin layer has been experimentally fabricated on various substrates [59,60]. The other layers of the TPV structure remain unchanged. Gap spacing d is 10 nm and the distance between the InAs cell and ITO emitter is thus 12 nm. The dielectric function of Pt is given by a Drude model $\varepsilon(\omega) = \varepsilon_\infty - \omega_p^2/(\omega^2 + i\omega\Gamma)$, where $\varepsilon_\infty = 5.4$, $\omega_p = 5.145$ eV, and $\Gamma = 0.069$ eV [61,62]. In evaluating such a modified system, it is critical to separate the absorption in the metal layer from that in the cell since only the absorption in the cell can be used to produce electricity. Here, we use dyadic Green's functions [50] together with the scattering matrix method [63] to obtain the transmission coefficients from the emitter to the Pt-covered InAs cell (including the Pt film) and only the InAs cell (excluding the Pt film).

Fig. 6(a) shows the spectral heat flux absorbed by the Pt and InAs cell as well as by only the InAs cell at the maximum electric power density when $d = 10$ nm and $T_1 = 900$ K. The Pt film induces substantial sub-bandgap heat transfer as suggested by the significant portion below the bandgap. Comparing Fig. 6(a) with Fig. 3, we note that the spectral heat flux peak due to SPhPs is suppressed by the covered Pt layer. The spectrum for the InAs cell has a very similar shape to the spectrum in Fig. 3 because the absorption in InAs still relies on interband transitions. Integrating the spectral heat flux in Pt and InAs cell yields a heat transfer rate of 561.8 W/cm², which is nearly 20-fold compared to the case without the Pt film shown in Fig. 3. About 13% of the total heat transfer (73.7 W/cm²) is absorbed in the InAs, yielding an electric power density of 31 W/cm². This value is nearly three times the maximum electric power density without the Pt film, though the efficiency becomes much lower to 5.5% because of the substantial absorption in the Pt film. This technique is valuable in waste heat recovery in those applications when one is primarily concerned with power density rather than efficiency.

The substantial increase of power density comes from the thermally excited plasmonic resonances in Pt film. Fig. 6(b) shows the transmission coefficient between the emitter and the Pt-covered InAs cell. The ITO SPP branch is still present but a new branch occurs in the lower frequency range. Similar to the SPPs on the interface of vacuum and ITO, SPPs can be thermally excited on the vacuum-Pt and the Pt-InAs interfaces. These two SPPs can couple and form two branches of coupled surface plasmon polaritons [51,64]. The relevant peak in Fig. 6(b) corresponds to the lower-frequency branch of these two coupled surface plasmons, as can be seen by comparing the location of the peaks in the ω-β plane to the dispersion relations of the SPPs from the vacuum-Pt and the Pt-InAs interfaces in the green dashed line [65]. The SPP branch due to platinum extends to very large β and hence greatly enhances the transmission coefficients at large β. This effect is further illustrated in Fig. 6(c), which shows the transmission coefficient between the emitter and the InAs cell. Compared to Fig. 4(a), the transmission of the large-β channels at the vicinity of the bandgap becomes higher as indicated by the brighter color. Therefore, we can conclude that a thin metal layer can indeed induce more absorption in the InAs cell. Recent works propose to use graphene covered semiconductor to improve the power density of near-field TPV may also be understood based on the above discussion since graphene can behave like a thin metallic layer [39,66].

We end our discussion by noting a possibility of harvesting the heat absorbed in the Pt film using Schottky junctions based on a recently proposed hot-carrier based technique [56]. In this way, additional electricity may be produced and the electric power density and efficiency of the current near-field TPV system may be further improved.
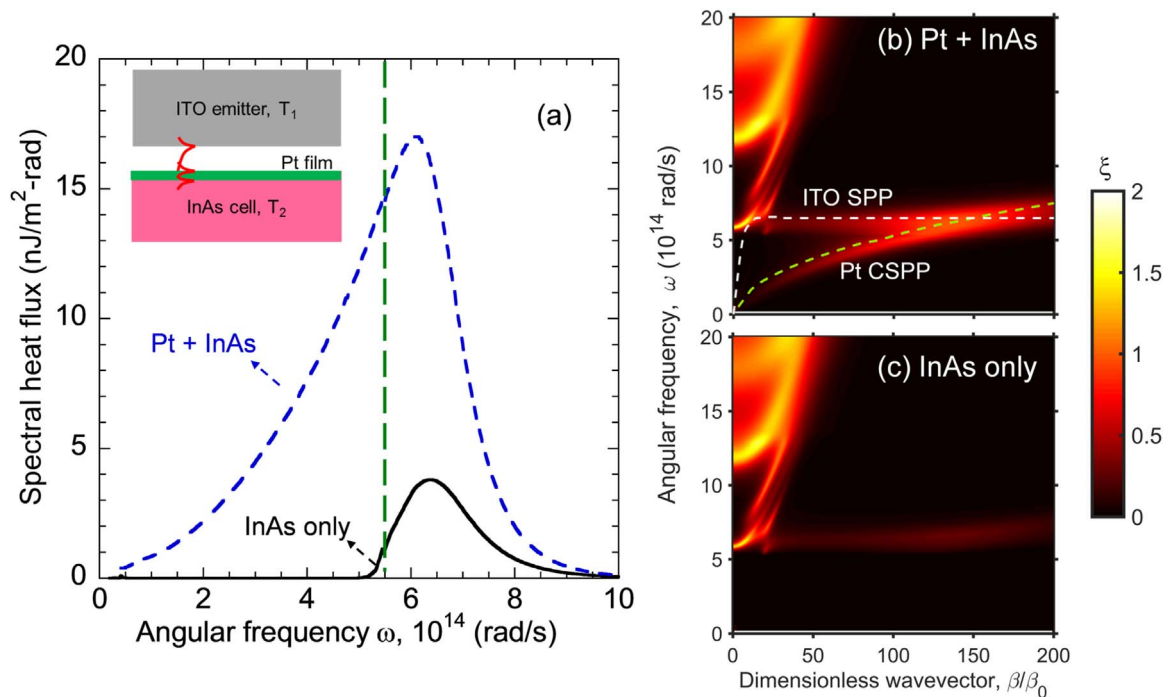
Fig. 6. (a) Spectral heat flux absorbed by both the Pt and the InAs cells, and by the InAs cell only at the maximum electric power density when $d = 10$ nm and $T_1 = 900$ K, for the configuration shown schematically in the inset where a thin Pt film is placed on top of the InAs cell. The vertical dashed line indicates the bandgap of InAs. (b) Transmission coefficient as a function of ω and β for Pt-covered InAs cell (including the Pt film). The white dashed line is the dispersion of the SPP on the ITO-vacuum interface and the green dashed line is the dispersion of the symmetric branch of the coupled SPP in Pt film with vacuum and InAs being the cladding materials. (c) Transmission coefficient as a function of ω and β for the InAs cell only (excluding the Pt film).

5. Conclusions

In conclusion, we reexamine the performance of the near-field TPV system using ITO and InAs for waste heat recovery applications. Infrared surface plasmons at the vacuum-ITO interface can be thermally excited and the near-field coupling effect reshapes and enhances the spectral heat transfer distribution toward the InAs cell. Based on a detailed balance analysis, we show that the system allows electricity generation with up to 40% efficiency and 11 W/cm² power density at a 900 K emitter temperature, even in the presence of nonradiative re-combination and the sub-bandgap heat transfer. Surface plasmon po-laritons play a dominant role, especially at small gap distances. A thin Pt layer can be used to cover the InAs cell to further boost the power density to 31 W/cm² by taking advantage of the thermally excited plasmon resonances in the thin metal film. The system is based on conventional thin films and thus can be scaled up in a straightforward manner. This work facilitates the understanding of near-field heat transfer at the nanoscale and demonstrates the great potential of using near-field TPVs for waste heat recovery applications.

Acknowledgement

References

[1] BCS, Inc., Waste Heat Recovery: Technology and Opportunities in U.S. Industry for the U.S. Department of Energy, Industrial Technologies Program, March, 2008.
[2] W. Liu, Q. Jie, H.S. Kim, Z. Ren, Acta Mater. 87 (2015) 357–376.
[3] F.R. Ovik, B.D. Long, M.C. Barma, M. Riaz, M.F.M. Sabri, S.M. Said, R. Saidur, Renew, Sustain. Energy Rev. 64 (2016) 635–659.
[4] B.D. Wedlock, Proc. IEEE 51 (1963) 694–698.
[5] H. Yugami, H. Sai, K. Nakamura, N. Nakagawa, H. Ohtsubo, Solar thermo-photovoltaic using Al₂O₃/Er₃Al₅O₁₂ eutectic composite selective emitter, in: Proceedings of the Conference Record of the Twenty-Eighth IEEE Photovoltaic Specialists Conference (Cat. No.00CH37036), 2000, pp. 1214–1217.
[6] A.S. Vlasov, V.P. Khvostikov, O.A. Khvostikova, P.Y. Gazaryan, S.V. Sorokina, V.M. Andreev, AIP Conf. Proc., 890, 2007, pp. 327–334.
[7] W.R. Chan, P. Bermel, R.C.N. Pilawa-Podgurski, C.H. Marton, K.F. Jensen, J.J. Senkevich, J.D. Joannopoulos, M. Soljačić, I. Celanovic, Proc. Natl. Acad. Sci. USA 110 (2013) 5309–5314.
[8] A. Datas, C. Algora, Prog. Photovolt. Res. Appl. 21 (2013) 1025–1039.
[9] A. Lenert, D.M. Bierman, Y. Nam, W.R. Chan, I. Celanovic, M. Soljačić, E.N. Wang, Nat. Nanotechnol. 9 (2014) 126–130.
[10] D.M. Bierman, A. Lenert, W.R. Chan, B. Bhatia, I. Celanović, M. Soljačić, E.N. Wang, Nat. Energy 1 (2016) 16068.
[11] J.-J. Greffet, R. Carminati, K. Joulain, J.-P. Mulet, S. Mainguy, Y. Chen, Nature 416 (2002) 61–64.
[12] J.M. Gee, J.B. Moreno, L. Shawn-Yu, J.G. Fleming, Selective emitters using photonic crystals for thermophotovoltaic energy conversion, in: Proceedings of the Conference Record of the Twenty-Ninth IEEE Photovoltaic Specialists Conference, 2002, pp. 896–899.
[13] F. O'Sullivan, I. Celanovic, N. Jovanovic, J. Kassakian, S. Akiyama, K. Wada, J. Appl. Phys. 97 (2005) 033529.
[14] I. Celanovic, N. Jovanovic, J. Kassakian, Appl. Phys. Lett. 92 (2008) 193101.
[15] E. Rephaeli, S. Fan, Opt. Express 17 (2009) 15145–15159.
[16] P. Bermel, M. Ghebrebrhan, W. Chan, Y.X. Yeng, M. Araghchini, R. Hamam, C.H. Marton, K.F. Jensen, M. Soljacic, J.D. Joannopoulos, S.G. Johnson, I. Celanovic, Opt. Express 18 (2010) A314–A334.
[17] V. Rinnerbauer, S. Ndao, Y.X. Yeng, W.R. Chan, J.J. Senkevich, J.D. Joannopoulos, M. Soljacic, I. Celanovic, Energy Environ. Sci. 5 (2012) 8815–8823.
[18] M. De Zoysa, T. Asano, K. Mochizuki, A. Oskooi, T. Inoue, S. Noda, Nat. Photonics 6 (2012) 535–539.
[19] Y.X. Yeng, W.R. Chan, V. Rinnerbauer, J.D. Joannopoulos, M. Soljačić, I. Celanovic, Opt. Express 21 (2013) A1035–A1051.
[20] B. Zhao, L.P. Wang, Y. Shuai, Z.M. Zhang, Int. J. Heat Mass Transf. 67 (2013) 637–645.
[21] Z. Zhou, Q. Chen, P. Bermel, Energy Convers. Manag. 97 (2015) 63–69.
[22] S.M. Rytov, Y.A. Kravtsov, V.I. Tatarskii, Principles of Statistical Radiophysics,

Springer, New York, 1989.
[23] A. Kittel, W. Muller-Hirsch, J. Parisi, S.A. Biehs, D. Reddig, M. Holthaus, Phys. Rev. Lett. 95 (2005) 224301.
[24] E. Rousseau, A. Siria, G. Jourdan, S. Volz, F. Comin, J. Chevrier, J.J. Greffet, Nat. Photon. 3 (2009) 514–517.
[25] S. Shen, A. Narayanaswamy, G. Chen, Nano Lett. 9 (2009) 2909–2913.
[26] S. Basu, B.J. Lee, Z.M. Zhang, J. Heat Transf. 132 (2010) 023302.
[27] R. St-Gelais, B. Guha, L. Zhu, S. Fan, M. Lipson, Nano Lett. 14 (2014) 6971–6975.
[28] B. Song, Y. Ganjeh, S. Sadat, D. Thompson, A. Fiorino, V. Fernández-Hurtado, J. Feist, F.J. Garcia-Vidal, J.C. Cuevas, P. Reddy, E. Meyhofer, Nat. Nanotechnol. 10 (2015) 253–258.
[29] M. Lim, S.S. Lee, B.J. Lee, Phys. Rev. B 91 (2015) 195136.
[30] J.I. Watjen, B. Zhao, Z.M. Zhang, Appl. Phys. Lett. 109 (2016) 203112.
[31] X. Liu, Z.M. Zhang, Nano Energy 26 (2016) 353–359.
[32] V. Fernández-Hurtado, F.J. García-Vidal, S. Fan, J.C. Cuevas, Phys. Rev. Lett. 118 (2017) 203901.
[33] R. St-Gelais, B. Guha, L. Zhu, S. Fan, M. Lipson, Nano Lett. 14 (2014) 6971–6975.
[34] R. St-Gelais, L. Zhu, S. Fan, M. Lipson, Nat. Nanotechnol. 11 (2016) 515–519.
[35] B. Song, D. Thompson, A. Fiorino, Y. Ganjeh, P. Reddy, E. Meyhofer, Nat. Nanotechnol. 11 (2016) 509–514.
[36] A. Narayanaswamy, G. Chen, Appl. Phys. Lett. 82 (2003) 3544–3546.
[37] M. Laroche, R. Carminati, J.J. Greffet, J. Appl. Phys. 100 (2006) 063704–063710.
[38] K. Park, S. Basu, W.P. King, Z.M. Zhang, J. Quant. Spectrosc. Radiat. Transf. 109 (2008) 305–316.
[39] R. Messina, P. Ben-Abdallah, Sci. Rep. 3 (2013) 1383.
[40] T.J. Bright, L.P. Wang, Z.M. Zhang, J. Heat Transf. 136 (2014) (062701-062701-062709).
[41] J.K. Tong, W.-C. Hsu, Y. Huang, S.V. Boriskina, G. Chen, Sci. Rep. 5 (2015) 10661.
[42] S. Molesky, Z. Jacob, Phys. Rev. B 91 (2015) 205435.
[43] W.-C. Hsu, J.K. Tong, B. Liao, Y. Huang, S.V. Boriskina, G. Chen, Sci. Rep. 6 (2016) 34837.
[44] A. Karalis, J.D. Joannopoulos, Sci. Rep. 6 (2016) 28472.
[45] J.I. Watjen, X.L. Liu, B. Zhao, Z.M. Zhang, J. Heat Transf. 139 (2017) (052704-052704-052708).
[46] O. Ilic, M. Jablan, J.D. Joannopoulos, I. Celanovic, M. Soljačić, Opt. Express 20 (2012) A366–A384.
[47] W. Shockley, H.J. Queisser, J. Appl. Phys. 32 (1961) 510–519.
[48] K. Chen, P. Santhanam, S. Sandhu, L. Zhu, S. Fan, Phys. Rev. B 91 (2015) 134301.
[49] S. Krishnamurthy, M.A. Berding, J. Appl. Phys. 90 (2001) 848–851.
[50] D. Polder, M. Van Hove, Phys. Rev. B 4 (1971) 3303–3314.
[51] Z.M. Zhang, Nano/Microscale Heat Transfer, McGraw-Hill, New York, 2007.
[52] X.L. Liu, R.Z. Zhang, Z.M. Zhang, Int. J. Heat Mass Transf. 73 (2014) 389–398.
[53] E.D. Palik, Handbook of Optical Constants of Solids, Academic Press, San Diego, CA, 1985.
[54] G.V. Naik, J. Kim, A. Boltasseva, Opt. Mater. Express 1 (2011) 1090–1099.
[55] O.J. Gregory, Q. Luo, E.E. Crisman, Thin Solid Films 406 (2002) 286–293.
[56] R. St-Gelais, G.R. Bhatt, L. Zhu, S. Fan, M. Lipson, ACS Nano 11 (2017) 3001–3009.
[57] R. He, D. Kraemer, J. Mao, L. Zeng, Q. Jie, Y. Lan, C. Li, J. Shuai, H.S. Kim, Y. Liu, D. Broido, C.-W. Chu, G. Chen, Z. Ren, Proc. Natl. Acad. Sci. USA 113 (2016) 13576–13581.
[58] A. Karalis, J.D. Joannopoulos, M. Soljačić, Phys. Rev. Lett. 103 (2009) 043906.
[59] L. Baker, A.S. Cavanagh, J. Yin, S.M. George, A. Kongkanand, F.T. Wagner, Appl. Phys. Lett. 101 (2012) 111601.
[60] T. Aaltonen, M. Ritala, T. Sajavaara, J. Keinonen, M. Leskelä, Chem. Mater. 15 (2003) 1924–1928.
[61] M.A. Ordal, R.J. Bell, R.W. Alexander, L.L. Long, M.R. Querry, Appl. Opt. 24 (1985) 4493–4499.
[62] H. Gai, J. Wang, Q. Tian, Appl. Opt. 46 (2007) 2229–2233.
[63] D.M. Whittaker, I.S. Culshaw, Phys. Rev. B 60 (1999) 2610–2618.
[64] E. Economou, Phys. Rev. 182 (1969) 539.
[65] H. Raether, Surface Plasmons on Smooth and Rough Surfaces and on Gratings, Springer-Verlag, Berlin, 1988.
[66] M. Lim, S. Jin, S.S. Lee, B.J. Lee, Opt. Express 23 (2015) A240–A253.

Kaifeng Chen received his B.S. degree from University of Science and Technology of China in 2013. He had an M.S. degree in Electrical Engineering from Stanford University in 2015. He is currently a Ph.D. candidate in Applied Physics department at Stanford University working with Professor Shanhui Fan. His research focuses on the active control of near-field heat transfer and Casimir force using non-zero chemical potential for photons, and numerical algorithms for electromagnetic simulations.

Siddharth Buddhiraju received his B. Tech. and M. Tech. degrees from the Indian Institute of Technology Bombay, India in 2015. He is currently a Ph.D. candidate in Department of Electrical Engineering at Stanford University in the research group of Professor Shanhui Fan. His research focuses on theoretical calculations and numerical simulations for solar, thermal and near-field heat transfer applications.

Gaurang Bhatt received his B. Eng. from Sardar Patel University, India in 2008. He obtained his M.S. degree in Electrical Engineering from Indian Institute of Technology Madras, India in 2012. He is currently a doctoral student working with Professor Michal Lipson at Columbia University. His research focuses on nano-photonics, plasmonics and radiative heat transfer in near- and far-field.

Michal Lipson received her B.S., M.S., and Ph.D. degrees in Physics at the Technion in 1998. She joined the School of Electrical and Computer Engineering at Cornell University in 2001. She is a MacArthur fellow and currently Eugene Higgins Professor of Electrical Engineering at Columbia University. Her research focuses on silicon photonics, new materials, and novel physical phenomena of light impacting areas in communication, biology and energy transfer.

Shanhui Fan received his Ph.D. in theoretical condensed matter physics from the Massachusetts Institute of Technology in 1997. He is currently a Professor of Electrical Engineering, and the Director of the Edward L. Ginzton Laboratory, at Stanford University. His research focuses on fundamental studies of nanophotonic structures, and the applications of these structures in various technologies including energy and information technology.
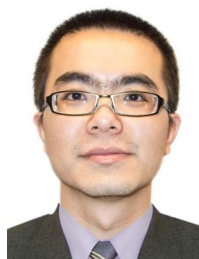
Bo Zhao received his B.S. degree in from University of Science and Technology of China in 2011. He worked with Professor Zhuomin Zhang and obtained his Ph.D. degree in Mechanical Engineering at Georgia Institute of Technology in 2016. He is now a postdoctoral research associate working with Professor Shanhui Fan at Stanford University. His research focuses on thermal photonics, near- and far-field thermal radiation, plasmonics, and radiative properties of 2D materials.